

Unsupervised Anomaly Detection and Localisation with Multi-scale Interpolated Gaussian Descriptors

Yuanhong Chen^{1*} Yu Tian^{1,2*} Guansong Pang¹ Gustavo Carneiro¹

¹ Australian Institute for Machine Learning, University of Adelaide

² South Australian Health and Medical Research Institute

Abstract

Current unsupervised anomaly detection and localisation systems are commonly formulated as one-class classifiers that depend on an effective estimation of the distribution of normal images and robust criteria to identify anomalies. However, the distribution of normal images estimated by current systems tends to be unstable for classes of normal images that are under-represented in the training set, and the anomaly identification criteria commonly explored in the field does not work well for multi-scale structural and non-structural anomalies. In this paper, we introduce an unsupervised anomaly detection and localisation method designed to address these two issues. More specifically, we introduce a normal image distribution estimation method that is robust to under-represented classes of normal images – this method is based on adversarially interpolated descriptors from training images and a Gaussian classifier. We also propose a new anomaly identification criterion that can accurately detect and localise multi-scale structural and non-structural anomalies. In extensive experiments on MNIST, Fashion MNIST, CIFAR10 and MVTec AD data sets, our approach shows better results than the current state of the arts in the standard experimental setup for unsupervised anomaly detection and localisation. Code is available at <https://github.com/tianyu0207/IGD>.

1. Introduction

Anomaly detection and localisation have been an active field of research in medical imaging [41, 63, 64, 70], surveillance [25, 28, 39, 43, 55, 56, 67, 80, 84, 86], and traffic anomaly detection [47, 78, 80]. We focus on the problem of detecting and localising anomalies in images, where the objectives can be summarised as follows: 1) estimate the probability that an image contains an anomaly, and 2)

localise the anomaly within an anomalous image. Given that most of the training sets available only contain normal images, methods are usually formulated as one-class classifiers (OCC) [25, 28, 39, 43, 54–56, 73, 84] – these methods are commonly referred to as unsupervised anomaly detectors. The functionality of OCCs depends on the robustness of the learned distribution of normal images to under-represented classes of normal images. OCCs also rely on the effectiveness of a criterion to identify multi-scale structural and non-structural anomalies within an image. Hence, these two points have been intensively studied in the literature.

When the learned distribution of normal images [21, 53, 60] does not generalise well, it cannot represent classes of unseen normal images that are under-represented in the training set, resulting in false detection of anomalies. Methods to constrain the distribution of normal images to lie at specific regions of the feature space have been proposed to mitigate this issue [53, 60], but they still do not provide a robust generalisation, as evidenced by their results. A recent trend in the field to address this generalisation issue is the use of self-supervision [6, 20]. Although successful in synthetic anomaly detection problems, such as CIFAR10 [33], they show poor generalisation in real-world data sets, such as MVTec AD [7], and they also have training and testing procedures of significantly higher run-time complexities than competing approaches [8, 21, 34, 73]. Moreover, all of the above self-supervised approaches do not work well for unsupervised anomaly localisation tasks.

The criteria to identify an anomalous image, and localise the anomaly within an image, are usually based on the reconstruction loss between the original image and its reconstructed image obtained from a generative model fitted to represent the normal training data [21, 30, 39, 46, 48, 58, 61, 62, 82]. Such reconstruction loss generally relies on the mean square error (MSE), which can miss multi-scale structural anomalies [49, 76]. Recently, a method based on structural similarity index measure (SSIM) [76] has been proposed [9] to detect single-scale structural anomalies, but anomalies can exhibit abnormality in varying scales, as

*First two authors contributed equally to this work.

†Corresponding author.

shown in Fig. 2.

In this paper, we introduce a novel unsupervised anomaly detection and localisation method that tackles the issues described above. We propose a new method to learn the robust distribution of normal images by our proposed interpolated Gaussian descriptor (IGD), which is a synthesis of the adversarially constrained auto-encoder interpolation (ACAI) [10] and a Gaussian classifier-enabled Support Vector Data Descriptor (GSVDD) model. The interpolated features produced by ACAI combined with the expectation maximisation (EM) optimisation of GSVDD intensify the feature representation learning for the under-represented normal images in the training set, resulting in substantially improved robustness w.r.t. these under-represented images. Moreover, we introduce a novel criterion to identify anomalous images and localise the anomalous regions based on the multi-scale structural similarity index measure (MS-SSIM) [76, 77], which is shown to accurately identify structural and non-structural anomalies of varying sizes. We evaluate our framework on MNIST [35], Fashion MNIST (FMNIST) [81] CIFAR10 [33] and MVTec AD [7]. On the real-world data set MVTec AD [7], our method shows the best detection and localisation results in the field. For the synthetic problems on MNIST, CIFAR10 and FMNIST, our method is the best with the standard experimental setup used in the field [8, 21, 34, 73].

2. Related Work

Unsupervised anomaly detection can be defined as a one-class classification problem that estimates the probability that an image is normal or anomalous, and anomaly localisation estimates the same probability, but at a pixel or image patch level. For both problems, we assume that the training set contains only normal images, which allows the development of systems referred to as unsupervised anomaly detection and localisation.

2.1. Unsupervised Anomaly Detection

Unsupervised anomaly detection is generally solved with one-class classification (OCC) [66] that clusters the features extracted from normal training images around a particular region of the feature space, and classification is based on how close image features are from this region. Initially, OCCs were explored with hand-crafted features [4, 45, 75, 83], but more recently, end-to-end deep learning models that learn both the feature extractor and classifier have been proposed [1, 6, 8, 13, 16, 20, 44, 46, 50, 50, 53, 60, 62, 69, 73, 74, 87]. A representative model of these approaches is the SVDD [69], which forces all normal image features to be inside a hyper-sphere with a pre-defined centre and a radius that is minimised to contain all training images. Then, test images that fall inside the learned hyper-sphere are classified as normal, and the ones outside are anomalous. Al-

though powerful, the hard boundary of SVDD can cause the model to overfit the training data.

Such hard decision boundary was addressed by Ruff et al. [60] with a soft-margin SVDD, but their optimisation fails to optimise the latent variables, leading to a sub-optimal solution. Alternatively, this was also solved with generative models, such as the generative adversarial network (GAN) [53] and auto-encoders (AE) [12, 21, 30, 30, 39, 46, 48, 48, 48, 50, 58, 61, 62, 73, 82, 88]. In [53], a GAN is trained to produce normal samples, and its discriminator is used to detect anomalies, but the hard training process of GANs represents a disadvantage of this approach. Alternatively, AE can be trained to reconstruct normal data, and the anomaly score is defined as the reconstruction error between the input and reconstructed images. These AE approaches depend heavily on the reconstruction loss, where MSE loss produces detectors that tend miss anomalous images containing structural anomalies, while single-scale SSIM loss [9] tends to work poorly for non-structural anomalies and structural anomalies of sizes outside that single scale.

The robustness of anomaly detectors can be improved if they are fine-tuned from models pre-trained on other tasks, such as image classification [49, 73], video understanding [67, 71, 74, 80, 86], and object detection [30]. Venkataramanan et al. [73] utilise a model pre-trained on ImageNet [18] and CelebA [42] as the backbone of encoder and discriminator, respectively, and they show promising results on different anomaly detection benchmarks. The state-of-the-art (SOTA) model by Bergmann et al. [8] uses a student-teacher framework to predict anomalies with multiple shallow students to regress the output of teacher network, which has prior knowledge from a complex network pre-trained on ImageNet. Given the positive results obtained by [8], we also rely on knowledge distillation to pre-train our method.

Recent works [6, 20] use self-supervised training to increase the effectiveness of the learned embeddings for the detection of anomalies. This self-supervision is achieved by predicting the type of transformations present in the data augmentation of input images. For instance, GeoTrans [20] trains a classifier to predict the geometric transformation applied to normal training data, and combines the prediction of each type of transformation as the anomaly score for transformed testing images. Bergman et al. [6] extend SVDD [60] to construct a hyper-sphere for each type of data augmentation. During testing, they predict the probability that all transformed samples fall into their respective hyper-spheres. Although self-supervised learning presents good anomaly detection results, there is no evidence that these approaches can localise anomalies given that the results on real-world anomaly detection data sets, like MVTec [7], are well below the SOTA. It appears that self-supervised learn-

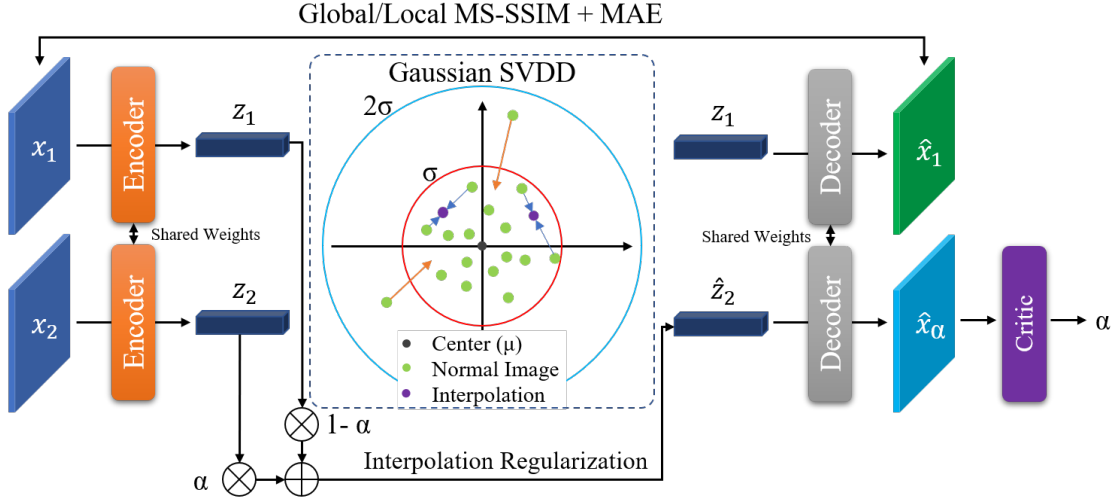


Figure 1. Overview of our proposed framework. The pipeline includes a deep AE to learn to reconstruct normal images with a MS-SSIM and MAE losses, and a Gaussian SVDD module to map the normal training images to be close to the mean of a Gaussian distribution, which is learned by training a critic network to uncover the mixing up coefficient α that produces a convex combination of the features of training samples.

ing is effective only in data sets where the anomaly is represented by the whole image (e.g., a dog image is an anomaly for a system trained with “normal” cat images), such as CIFAR10. Moreover, self-supervised learning increases significantly the running time of the training and testing processes, with a typical increase of 10-fold in both processes – in fact, self-supervised methods rely on a different experimental setup than the one used on several benchmarks, which uses a large amount of data augmentation during training and testing. Given that we aim to produce SOTA detection and localisation results on real-world data sets, we do not rely on self-supervised learning.

2.2. Unsupervised Anomaly Localisation

Unsupervised anomaly localisation targets the segmentation of anomalous image pixels or patches, containing, for example, lesions from medical images [36, 40], defects in industry images [7, 8], and anomalies in traffic images [52]. The main idea explored is based on extending the image based OCC to a pixel-based OCC. Then, testing produces a pixel-wise anomaly score map, where a pixel with a high score represents an anomalous pixel [2, 5, 9, 57, 64]. The way such scores are computed are based on the same anomaly detection criteria presented above in Sec. 2.1. In general, methods that can localise anomalies [8, 63, 73] are tuned to particular anomaly sizes and structure, which can cause then to miss anomalies outside that range of sizes and structure.

3. Method

Our method assumes the availability of a training set that contains only normal samples and is denoted by $\mathcal{D} = \{\mathbf{x}_i\}_{i=1}^{|\mathcal{D}|}$, where $\mathbf{x} \in \mathcal{X} \subset \mathbb{R}^{W \times H \times 3}$ represents an RGB image of width W and height H . The testing set contains normal and anomalous images, where anomalous images have segmentation map annotations. This testing set is defined by $\mathcal{T} = \{(\mathbf{x}_i, y_i, \mathbf{b}_i^{(y_i)})\}_{i=1}^{|\mathcal{T}|}$, where $y_i \in \mathcal{Y} = \{\text{normal, anomalous}\}$ and the segmentation map with the anomaly is denoted by $\mathbf{b}_i^{(y_i)} \in \{0, 1\}^{W \times H}$ (0 denotes a normal and 1 denotes an anomalous pixel in the image \mathbf{x}_i), if $y_i = \text{anomalous}$, and $\mathbf{b}_i^{(y_i)} = 0^{W \times H}$ if $y_i = \text{normal}$.

Our proposed model is defined by an auto-encoder (see Fig. 1) that reconstructs an input image with

$$\tilde{\mathbf{x}} = g_\phi(f_\theta(\mathbf{x})), \quad (1)$$

where $f_\theta : \mathcal{X} \rightarrow \mathcal{Z}$ represents the encoder that takes an image $\mathbf{x} \in \mathcal{X}$ and produces an embedding $\mathbf{z} \in \mathcal{Z} \subset \mathbb{R}^{d_z}$ using an encoder parameterised by θ , representing the network weights; and $g_\phi : \mathcal{Z} \rightarrow \mathcal{X}$ denotes the decoder parameterised by ϕ , which transforms an embedding $\mathbf{z} \in \mathcal{Z}$ to an image $\mathbf{x} \in \mathcal{X}$. The training process is regularised by the learning of a critic network (see Fig. 1) that estimates the amount of convex combination $\alpha \in [0, 0.5]$ between two input embeddings, as follows

$$\tilde{\alpha} = d_\psi(g_\phi(\alpha f_\theta(\mathbf{x}_1) + (1 - \alpha) f_\theta(\mathbf{x}_2))), \quad (2)$$

where d_ψ represents the critic network, and $\mathbf{x}_1, \mathbf{x}_2 \in \mathcal{X}$, with $\mathbf{x}_1 = \mathbf{x}$ and $f_\theta(\mathbf{x}_2)$ is obtained by reversing the order

of the elements along the length of the vector $f_\theta(\mathbf{x}_1)$ [10]. Our model also contains a Gaussian SVDD (GSVDD) anomaly classifier parameterised by $\gamma = \{\mu_\gamma, \sigma_\gamma\}$ (see Fig. 1), defined as

$$p_{GSVDD}(\text{anomalous}|\mathbf{x}, \gamma) = h_\gamma(f_\theta(\mathbf{x})). \quad (3)$$

The loss to train this model is defined by

$$\frac{1}{|\mathcal{D}|} \sum_{i=1}^{|\mathcal{D}|} (\ell_d(\mathbf{x}_i) + \ell_{f,g}(\mathbf{x}_i) + \ell_h(\mathbf{x}_i)), \quad (4)$$

where $\ell_d(\cdot)$ is the loss for training the critic model, $\ell_{f,g}(\cdot)$ for the encoder and decoder models based on the MS-SSIM reconstruction loss, and $\ell_h(\cdot)$ for training the GSVDD model. Below we provide more detail for each loss, where our main contributions are: 1) the Interpolated Gaussian Descriptor (IGD) that combines the adversarially constrained auto-encoder interpolation (ACAI) [10] and an extension for the SVDD model [69] to work with a Gaussian classifier trained with the EM algorithm [17]; and 2) the use of MS-SSIM in the loss $\ell_{f,g}(\cdot)$ for training the encoder and decoder models.

3.1. Interpolated Gaussian Descriptor (IGD)

We train the anomaly classifier defined in (3) to produce results that are close to a pre-defined centre for images \mathbf{x} that belong to the same distribution as the images in \mathcal{D} , and push the embedding of anomalous image far from that distribution. Given that our training set \mathcal{D} contains only normal images, and that the size of this training set is limited, we propose the following strategy, named interpolated Gaussian descriptor (IGD), to train this classifier: 1) during training, we adapt the ACAI [10] loss to fill in the gaps between training samples in the embedding space produced by the encoder $f_\theta(\cdot)$ in (1); and 2) we replace the SVDD hyper-sphere with a Gaussian [60].

With ACAI, we aim to increase the robustness of the training by augmenting the data with convex combinations of training embeddings and also by a loss that penalises the incorrect estimation of the convex combination parameter. By replacing the hard SVDD constraint by a soft constraint based on the proposed Gaussian SVDD (GSVDD), we aim to make our model less sensitive to outliers present in \mathcal{D} , similarly to [60]. However, differently from [60], we train the GSVDD with the EM algorithm [17], where the mean and standard deviation of the Gaussian denote the latent variables. Our optimisation has better guarantees to reach a local optimum than the training by Ruff et al. [60] that does not update the latent variable estimation.

The loss to optimise the critic model in (4) is defined as [10]

$$\ell_d(\mathbf{x}) = \|d_\psi(\hat{\mathbf{x}}_\alpha) - \alpha\|_2^2 + \|d_\psi(\zeta\mathbf{x} + (1 - \zeta)g_\phi(f_\theta(\mathbf{x})))\|_2^2, \quad (5)$$

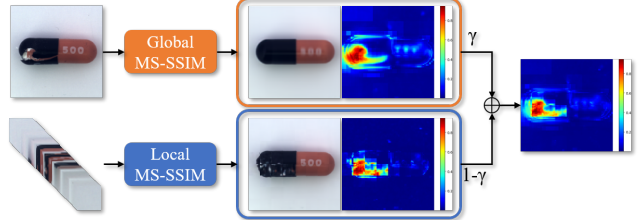


Figure 2. Example of the multi-scale structural and non-structural anomaly detection and localisation result for an MVTec AD [7] image, where both the local and global branches use the same MS-SSIM loss. Note that in this example, the global branch produces smooth results but with some mistakes, while the local branch produces jagged results, but without those mistakes, so by combining the two results, we obtain a smooth and correct anomaly heatmap.

where $\zeta \in [0, 1]$, $d_\psi(\cdot)$ is defined in (2), the encoder $f_\theta(\cdot)$ and decoder $g_\phi(\cdot)$ are defined in (1), and $\hat{\mathbf{x}}_\alpha = g_\phi(\alpha f_\theta(\mathbf{x}_1) + (1 - \alpha)f_\theta(\mathbf{x}_2))$. The optimisation of the encoder and decoder minimises the following loss

$$\ell_{f,g}(\mathbf{x}) = \ell_m(\mathbf{x}, \hat{\mathbf{x}}) + \lambda \|d_\psi(\hat{\mathbf{x}}_\alpha)\|_2^2, \quad (6)$$

where $\hat{\mathbf{x}} = g_\phi(f_\theta(\mathbf{x}))$ from (1), and the image reconstruction loss $\ell_m(\cdot)$ based on the MS-SSIM is defined below in (9). The GSVDD is optimised with the following loss:

$$\ell_h(\mathbf{x}) = 1 - h_\gamma(f_\theta(\mathbf{x})), \quad (7)$$

where $h_\gamma(f_\theta(\mathbf{x})) = \exp\left(-\frac{\|f_\theta(\mathbf{x}) - \mu_\gamma\|_2^2}{\sigma_\gamma^2}\right)$. The mean and standard deviation values above are estimated with $\mu_\gamma = \frac{1}{|\mathcal{D}|} \sum_{i=1}^{|\mathcal{D}|} f_\theta(\mathbf{x}_i)$ and $\sigma_\gamma^2 = \frac{\kappa}{|\mathcal{D}|} \sum_{i=1}^{|\mathcal{D}|} \|f_\theta(\mathbf{x}_i) - \mu_\gamma\|_2^2$, where $\kappa \in [0, 1]$ is a constant that regularises the estimation of σ_γ^2 to prevent numerical instabilities during training. The optimisation for the loss in (4) is based on the EM algorithm [17], where in the E-step, the latent variables μ_γ and σ_γ in (7) are estimated from the data using $f_\theta(\cdot)$, and in the M-step, we minimise the losses in (5), (6) and (7) to estimate the parameters of $f_\theta(\cdot)$, $g_\phi(\cdot)$ and $d_\psi(\cdot)$.

3.2. Detecting Structural and Non-structural Multi-scale Anomalies

Another contribution of our work is the introduction of a new criterion to detect multi-scale structural and non-structural anomalies – see Fig. 2. The idea of replacing MSE in anomaly detection problems [21, 30, 58, 73, 82] by SSIM [76] was proposed in [9], where the main argument is that MSE tends to be too brittle and produce high values when there are small localisation errors and it also fails to detect structural anomalies, represented by image abnormalities that have strong inter-dependencies between neighbouring pixels. We extend this idea in two ways: 1) we add the multi-scale extension of SSIM to form the MS-SSIM [77] that is more robust than its single-scale counterpart to varying localised anomaly scales; and 2) we optimise

this loss by combining the MS-SSIM loss using the whole image (global) and image regions (local).

The MS-SSIM loss ℓ_m in (6) combines a mean absolute error (MAE) loss with the MS-SSIM over the whole image and image patches, as follows:

$$\begin{aligned} \ell_m(\mathbf{x}, \tilde{\mathbf{x}}) = & \rho \sum_{\omega \in \Omega} \|\mathbf{x}_\omega - \tilde{\mathbf{x}}_\omega\|_1 + \\ & (1 - \rho) \sum_{\omega \in \Omega} 1 - (\beta m_G(\mathbf{x}_\omega, \tilde{\mathbf{x}}_\omega) + (1 - \beta)m_L(\mathbf{x}_\omega, \tilde{\mathbf{x}}_\omega)), \end{aligned} \quad (8)$$

where $\rho \in [0, 1]$, \mathbf{x}_ω is a patch from the original image \mathbf{x} of size $H_G \times W_G$ for the global and $H_L \times W_L$ for the local score of image patches, centred at pixel $\omega \in \Omega$ (Ω is the image lattice of size $H \times W$), $\tilde{\mathbf{x}}_\omega$ is the reconstruction of \mathbf{x}_ω from (1), and $\beta \in [0, 1]$ represents a hyper-parameter to produce a convex combination of the global and local scores. Also in (8), $m_G(\cdot), m_L(\cdot) \in [-1, +1]$ denote the global and local MS-SSIM scores, where the global score is defined as [77]

$$\begin{aligned} m_G(\mathbf{x}_\omega, \tilde{\mathbf{x}}_\omega) = & \\ [l_M(\mathbf{x}_\omega, \tilde{\mathbf{x}}_\omega)]^{\alpha_M} \prod_{m=1}^{M_G} & [c_m(\mathbf{x}_\omega, \tilde{\mathbf{x}}_\omega)]^{\beta_m} [s_m(\mathbf{x}_\omega, \tilde{\mathbf{x}}_\omega)]^{\gamma_m} \end{aligned} \quad (9)$$

where M_G denotes the number of scales for the global and local MS-SSIM, $\alpha_M, \beta_m, \gamma_m$ represent constants, $l_M(\mathbf{x}_\omega, \tilde{\mathbf{x}}_\omega) = \frac{2\mu_{\mathbf{x}_\omega}\mu_{\tilde{\mathbf{x}}_\omega} + C_1}{\mu_{\mathbf{x}_\omega}^2 + \mu_{\tilde{\mathbf{x}}_\omega}^2 + C_1}$, $c_m(\mathbf{x}_\omega, \tilde{\mathbf{x}}_\omega) = \frac{2\sigma_{\mathbf{x}_\omega}\sigma_{\tilde{\mathbf{x}}_\omega} + C_2}{\sigma_{\mathbf{x}_\omega}^2 + \sigma_{\tilde{\mathbf{x}}_\omega}^2 + C_2}$, $s_m(\mathbf{x}_\omega, \tilde{\mathbf{x}}_\omega) = \frac{\sigma_{\mathbf{x}_\omega}\sigma_{\tilde{\mathbf{x}}_\omega} + C_3}{\sigma_{\mathbf{x}_\omega}\sigma_{\tilde{\mathbf{x}}_\omega} + C_3}$, with C_1, C_2, C_3 representing pre-defined constants, $\mu_{\mathbf{x}_\omega}$ denoting the mean intensities of \mathbf{x}_ω , $\sigma_{\mathbf{x}_\omega}^2$ the variance of \mathbf{x}_ω , and $\sigma_{\mathbf{x}_\omega}\sigma_{\tilde{\mathbf{x}}_\omega}$ the covariance of \mathbf{x}_ω and $\tilde{\mathbf{x}}_\omega$. The local score m_L is defined in the same way as in (9).

3.3. Training and Inference

The training of our model starts with knowledge distillation pre-training, which has shown promising results on different problems [8, 22, 29]. In particular, we train an encoder of the same structure as in (1) with Imagenet [18], which forms $f_{\theta(I)}(\mathbf{x})$ – this is done with the cross entropy loss to train a classifier for the 10^3 classes using 10^6 images. We then pre-train the encoder $f_\theta(\cdot)$ in (1) using the images from \mathcal{D} to approximate the embeddings produced by the Imagenet model $f_{\theta(I)}(\cdot)$ using the following loss:

$$\ell_{KD} = \frac{1}{|\mathcal{D}|} \sum_{i=1}^{|\mathcal{D}|} \|f_{\theta(I)}(\mathbf{x}_i) - f_\theta(\mathbf{x}_i)\|_2^2. \quad (10)$$

As mentioned before, our training follows an EM optimisation, with the E-step consisting of estimating the values of the latent variables μ_γ and σ_γ in (7). For the M-step,

we minimise the loss in (4) by optimising θ with respect to $\ell_{f,g}(\cdot)$ in (6) and $\ell_h(\cdot)$ in (7), ϕ with respect to $\ell_{f,g}(\cdot)$ in (6) and ψ with respect to $\ell_d(\cdot)$ in (5).

During inference, **anomaly detection** is performed with the anomaly score of a testing image \mathbf{x} is:

$$s(\mathbf{x}) = \xi \ell_m(\mathbf{x}, \tilde{\mathbf{x}}) + (1 - \xi) \ell_h(\mathbf{x}), \quad (11)$$

where $\ell_m(\cdot)$ is the reconstruction loss in (8), $\tilde{\mathbf{x}} = f_\theta(\mathbf{x})$ as in (1), $\ell_h(\cdot)$ is the GSVDD loss in (7), and $\xi \in [0, 1]$ is a hyper-parameter. **Anomaly localisation** is obtained from the same loss as in (11), but computing for just a single image pixel $\omega \in \Omega$ with

$$\begin{aligned} \ell_m(\mathbf{x}_\omega, \tilde{\mathbf{x}}_\omega) = & \rho \|\mathbf{x}_\omega - \tilde{\mathbf{x}}_\omega\|_1 + \\ & (1 - \rho) (1 - (\beta m_G(\mathbf{x}_\omega, \tilde{\mathbf{x}}_\omega) + (1 - \beta)m_L(\mathbf{x}_\omega, \tilde{\mathbf{x}}_\omega))), \end{aligned} \quad (12)$$

with all terms as defined in (8). As shown in Fig. 2, this anomaly localisation creates a heatmap with high values representing regions that are likely to contain anomalies.

4. Experiments

4.1. Datasets and Evaluation Metric

Datasets: We use four different datasets to evaluate our methods, namely MNIST [35], Fashion MNIST [81], CIFAR10 [33] and MVTec AD [7]. MNIST, Fashion MNIST and CIFAR10 have been widely used as benchmarks for image anomaly detection, and we follow the same experimental protocol as described in [1, 8, 14, 21, 53, 60, 73]. CIFAR10 contains 60,000 images with 10 classes. MNIST and Fashion MNIST contains 70,000 images with 10 classes of handwritten digits and fashion product, respectively.

MVTec AD [7] is a recently released data set that contains 5,354 high-resolution real-world images of 15 different industry object and textures. The normal class of MVTec AD is formed by the images without defect anomalies and consists of 3,629 images for training and 467 images for testing. The anomalous class consists over 70 categories of defects (such as dents, structural fails, contamination, etc.) and contains 1,258 images. Furthermore, MVTec AD also provides pixel-wise ground truth annotations for all anomalies, allowing the evaluation of not only the anomaly detection, but also the anomaly localisation.

Evaluation Metric: For anomaly detection, similarly to [1, 8, 14, 21, 53, 60, 73], we use area under the receiver operating characteristic curve (AUC) as the evaluation metric for all data sets. On MNIST, Fashion MNIST and CIFAR10, we use the same protocol as [1, 6, 8, 20, 53, 60, 73], where training uses a single class as the normal data, with the nine remaining classes denoting the anomalous data, and inference relies on a non-augmented test image. We report the mean AUC over the 10 classes for the above three

Classifier	Method	MNIST	CIFAR10	FMNIST
Single	DAE [24]	0.8766	0.5358	-
	VAE [32]	0.9696	0.5833	-
	KDE [11]	0.8140	0.6100	-
	OCSVM [65]	0.9510	0.5860	-
	AnoGAN [64]	0.9127	0.6179	-
	DSVDD [60]	0.9480	0.6481	0.9280
	OCGAN [53]	0.9750	0.6566	-
	PixelCNN [72]	0.6180	0.5510	-
	CapsNetpp [37]	0.9770	0.6120	0.7650
	CapsNet _{RE} [37]	0.9250	0.5310	0.6790
	ADGAN [14]	0.9680	0.6340	-
	LSA [1]	0.9750	0.6410	0.8760
	MemAE [21]	0.9751	0.6088	-
	GradCon [34]	0.9730	0.6640	-
	λ -VAE _u [15]	0.9820	0.7170	0.8730
	ULSLM [79]	0.9490	0.7360	-
	CAVGA-D _u [73]	0.9860	0.7370	0.8850
	Ours	0.9912	0.8234	0.9332
Ensemble	Student-Teacher [8]	0.9935	0.8196	-
	Ours	0.9927	0.8368	0.9357

Table 1. **Anomaly detection:** mean AUC results on MNIST, CIFAR10 and Fashion MNIST. The results are split into single (top) and ensemble of five classifiers (bottom). Bold numbers represent the best result (within 1%) for each data set, discriminated by single or ensemble.

data sets. On MVTec AD, as suggested in [8, 73], we evaluate anomaly detection performance not only with AUC, but also with mean accuracy.

For anomaly localisation, we follow [73] to compute the mean pixel-level AUC between generated heatmap and the ground truth segmentation map for each anomalous image in the testing set on MVTec AD.

4.2. Implementation Details

We implement our framework using Pytorch [51]. The model was trained with Adam optimiser [31] using a learning rate of 0.0001, which decays to 0 over a pre-defined maximum number of epochs (with a polynomial function), weight decay of 10^{-6} , batch size of 64 images, 128 epochs for MNIST, Fashion MNIST and CIFAR 10, and 256 epochs for MVTec AD. We defined the latent space to have $d_z = 128$ dimensions in (1). For the remaining hyper-parameters, we randomly sampled α in (2) from the continuous uniform distribution in $[0, 0.5]$ [10], and set $\gamma = 0.2$ in (5) for the critic model, as suggested in [10]. The estimation of σ_γ^2 in (7) is lower bounded at 1 with $\kappa = 0.5$. The regularisation parameter λ in (6) is set to 0.1 for all the experiments (this value for λ was set based on the convergence of the critic network). We defined the global MS-SSIM to have $M_G = 5$ scales in (9) with weights $\beta_1 = \gamma_1 = 0.0448$, $\beta_2 = \gamma_2 = 0.2856$, $\beta_3 = \gamma_3 = 0.3001$, $\beta_4 = \gamma_4 = 0.2363$, $\alpha_5 = \beta_5 = \gamma_5 = 0.1333$ [77]. We follow $C_i = (K_i L)^2$ according to [76] and define $L = 4.7579$ as the pixel range with $K_1 = 0.01$, $K_2 = 0.03$ and $C_3 = C_2/2$. For the local MS-SSIM, we have $M_L = 4$ scales with weights

$\beta_1 = \gamma_1 = 0.0516$, $\beta_2 = \gamma_2 = 0.3295$, $\beta_3 = \gamma_3 = 0.3463$, $\alpha_4 = \beta_4 = \gamma_4 = 0.2726$ modified based on the original proportion for $M_G = 5$. Following [19, 85], we set $\rho = 0.15$ to balance the contribution of MAE and glocal MS-SSIM loss in (8). For MVTec AD, we set $\beta = 0.1$ in (8) and (12), since it shows the lowest anomaly score for normal samples on validation set¹. During inference, we set $\xi = 0.5$ in (11) based on the evaluation on the validation set.

For the local model in (8) and (12), the input image size is 32×32 (i.e., $H_L = W_L = 32$), where the encoder, decoder and critic models use three pre-activated [23] residual blocks (with each block containing two 3×3 convolution layers after batch normalisation and ReLU [27]). From first to last residual block, the encoder and critic models have 128–256–512 filters, and the decoder has 256–128–64 filters. For the global model in (8) and (12), the input image size is 256×256 (i.e., $H_G = W_G = 256$ – this means that $\ell_m(\cdot)$ in (8) is computed only at the centre pixel), where the encoder and critic consist of four residual blocks, with each block containing 512–256–128–64 and 128–256–512–512 filters, respectively. For the knowledge distillation pre-training process in (10), we follow [8] and compute the l_2 difference between the 512-dimensional feature vector output from encoder and an intermediate layer of a pre-trained ResNet18 [26] with the same 512-dimensional features. For this pre-training, we use the Adam optimiser with a learning rate of 0.0001, weight decay 10^{-5} , batch size of 64, and 50,000 iterations. Once we obtain the pre-trained encoder, we fix the network parameters and attach a linear layer to reduce the dimensionality of the feature space to 128.

4.3. Experiments on MNIST, Fashion MNIST and CIFAR10

Table 1 compares the unsupervised anomaly detection mean AUC results between our method and the current SOTA approaches in the field on MNIST, Fashion MNIST and CIFAR10. The rows labelled as “Single” show results of models using a single classifier, and the ones with “Ensemble” display results from models containing an ensemble of five classifiers [8]. Our approach outperforms all current SOTA methods even without model ensembling, and our ensemble classifier achieves comparable or better results than the teacher-student ensemble model by Bergmann et al. [8] on MNIST and CIFAR10. Note that CAVGA-D_u [73] uses ImageNet [18] and Celeb-A [42] pre-trained ResNet18 models for the encoder and discriminator, respectively, while ours only use a smaller network to distill the information from the ImageNet pre-trained ResNet18. It is also interesting to note that our approach based on the proposed GSVDD obtains a 4.47% and 18.87% improvement

¹This local MS-SSIM is not applied on MNIST, Fashion MNIST, and CIFAR10.

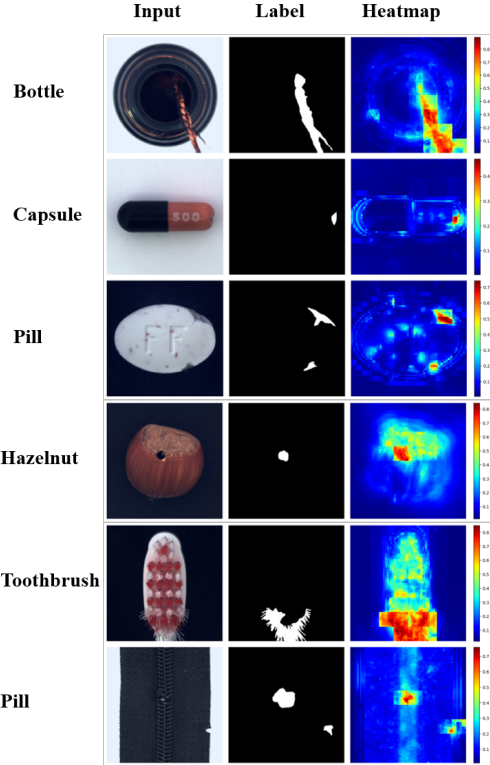


Figure 3. Illustration of the anomaly heatmaps produced by our model on MVTec AD (red = high probability of anomaly).

on MNIST and CIFAR10, when compared with the original DSVDD [60].

4.4. Experiments on MVTec AD

We report the results for both anomaly detection and localisation on MVTec AD, which contains real-world images of industry objects and textures containing different types of anomalies. We show the mean accuracy of anomaly detection in Tab. 2 over all image classes, where our model outperforms the previous SOTA methods CAVGA-D_u and CAVGA-R_u [73] by 6% and 2%, respectively. Our model achieves the best results in eight categories of the MVTec AD. The shallow generative baselines like DAE, AE-SSIM and AnoGAN yield sub-optimal results on MVTec AD. When compared with methods recently considered to be the MVTec AD SOTA, such as LSA [1] and λ -VAE_u [15], our approach shows more than 7% improvement. We further evaluate the anomaly detection mean AUC on MVTec AD, as shown in Tab. 3, where our method surpasses all previous methods by at least 2.8%, and produces the best results in nine categories.

For anomaly localisation, we compare our method and the SOTA using the mean pixel-level AUC of all anomalous images in the testing set of MVTec AD – see Tab. 4. Notice that our method is better than the previous SOTA

CAVGA-R_u [73] by 2%. It is also important to note that our architecture is lighter than CAVGA-R_u given that it does not use an attention module and a visual discriminator. Fig. 3 demonstrates the qualitative anomaly localisation results on MVTec AD images, where red regions in the heatmap indicate higher anomaly probability. From these results, we can see that our approach can localise anomalous regions of different sizes and structures from different object categories.

4.5. Ablation Studies

To investigate the effectiveness of each component of our method, we show an anomaly detection mean AUC ablation study on CIFAR10 in Tab. 5. The study starts with a model trained with the MS-SSIM reconstruction loss. This model already achieves a mean AUC of 68.52%, which is higher than the 55.38% AUC from DAE model, that relies on MSE as the reconstruction loss (see Tab. 1). After adding knowledge distillation (KD) and soft-boundary DSVDD [60], our model achieves a mean AUC of 73.1% and 79.5%, respectively. To show the importance of our proposed GSVDD, we replace the soft-boundary DSVDD with our GSVDD module, and the result indicates that GSVDD is 2.3% better. Finally, our proposed method including ACAI interpolation (INTER) improves the AUC by 0.49%. All the results in Tab. 5 rely on a model using a single classifier (i.e., no ensemble).

MS-SSIM	KD	DSVDD	GSVDD	INTER	AUC - CIFAR10
✓					0.685
✓	✓				0.731
✓	✓	✓			0.795
✓	✓		✓		0.819
✓	✓		✓	✓	0.823

Table 5. Ablation studies of our method on CIFAR10 using anomaly detection mean AUC (MS-SSIM: the backbone deep autoencoder with MS-SSIM loss, KD: knowledge distillation, DSVDD: soft-boundary Deep SVDD, GSVDD: our Gaussian SVDD, INTER: ACAI).

5. Discussion and Conclusion

In this paper, we presented a new unsupervised anomaly detection and localisation method which learns a distribution of normal images that generalises well to all classes of normal images, and a new criterion to detect and localise structural and non-structural multi-scale anomalies. Our learned distribution of normal images is based on the interpolated Gaussian descriptor (IGD) that provides a robust modelling of the normal image distribution with adversarially interpolated descriptors to train the proposed GSVDD. The proposed reconstruction loss can find structural and non-structural anomalies of varying sizes. Results show that our model achieves the best performance in the field on MNIST, CIFAR10, Fashion MNIST and MVTec AD in

Category	AVID [62]	AE _{SSIM} [9]	DAE [24]	AnoGAN [64]	λ -VAE _u [15]	LSA [1]	CAVGA-D _u [73]	CAVGA-R _u [73]	Ours
Bottle	0.85	0.88	0.80	0.69	0.86	0.86	0.89	0.91	0.96
Hazelnut	0.86	0.54	0.88	0.50	0.74	0.80	0.84	0.87	0.94
Capsule	0.85	0.61	0.62	0.58	0.86	0.71	0.83	0.87	0.83
Metal Nut	0.63	0.54	0.73	0.50	0.78	0.67	0.67	0.71	0.85
Leather	0.58	0.46	0.44	0.52	0.71	0.70	0.71	0.75	0.74
Pill	0.86	0.60	0.62	0.62	0.80	0.85	0.88	0.91	0.74
Wood	0.83	0.83	0.74	0.68	0.89	0.75	0.85	0.88	0.84
Carpet	0.70	0.67	0.50	0.49	0.67	0.74	0.73	0.78	0.79
Tile	0.66	0.52	0.77	0.51	0.81	0.70	0.70	0.72	0.92
Grid	0.59	0.69	0.78	0.51	0.83	0.54	0.75	0.78	0.77
Cable	0.64	0.61	0.56	0.53	0.56	0.61	0.63	0.67	0.81
Transistor	0.58	0.52	0.71	0.67	0.70	0.50	0.73	0.75	0.84
Toothbrush	0.73	0.74	0.98	0.57	0.89	0.89	0.91	0.97	0.93
Screw	0.66	0.51	0.69	0.35	0.71	0.75	0.77	0.78	0.78
Zipper	0.84	0.80	0.80	0.59	0.67	0.88	0.87	0.94	0.91
mean	0.73	0.63	0.71	0.55	0.77	0.73	0.78	0.82	0.84

Table 2. **Anomaly detection:** mean accuracy on MVTec AD produced by the SOTA and our method.

Category	AnoGAN [64]	GANomaly [2]	Skip-GANomaly [3]	U-Net [59]	DAGAN [68]	Ours
Bottle	0.800	0.794	0.937	0.863	0.983	0.998
Hazelnut	0.259	0.874	0.906	0.996	1.00	0.981
Capsule	0.442	0.721	0.718	0.673	0.687	0.884
Metal Nut	0.284	0.694	0.790	0.676	0.815	0.889
Leather	0.451	0.808	0.908	0.870	0.944	0.915
Pill	0.711	0.671	0.758	0.781	0.768	0.815
Wood	0.567	0.920	0.919	0.958	0.979	0.958
Carpet	0.337	0.821	0.795	0.774	0.903	0.799
Tile	0.401	0.720	0.850	0.964	0.961	0.971
Grid	0.871	0.743	0.657	0.857	0.867	0.823
Cable	0.477	0.711	0.674	0.636	0.665	0.901
Transistor	0.692	0.808	0.814	0.674	0.794	0.909
Toothbrush	0.439	0.700	0.689	0.811	0.950	0.986
Screw	0.100	1.000	1.000	1.000	1.000	0.748
Zipper	0.715	0.744	0.663	0.750	0.781	0.946
mean	0.503	0.782	0.805	0.819	0.873	0.901

Table 3. **Anomaly detection:** mean AUC on MVTec AD produced by the SOTA and our method.

Method	MVTec AD
DAE [24]	0.82
AE _{SSIM} [9]	0.87
AVID [62]	0.78
LSA [1]	0.79
λ -VAE _u [15]	0.86
AnoGAN [64]	0.74
ADVAE [38]	0.86
CAVGA-D _u [73]	0.85
CAVGA-R _u [73]	0.89
Ours	0.91

Table 4. **Anomaly localisation:** mean pixel-level AUC results on the anomalous images of MVTec AD.

terms of anomaly detection and localisation.

One point that remains to be investigated in this paper is the role that self-supervised learning can have in our model. This is important to study because recently proposed self-supervised anomaly detection methods show outstanding results on CIFAR10 (Bergman et al. [6] reports a 88.2%

mean AUC, and Golan et al. [20] reports 81.6% mean AUC on CIFAR10, respectively) and Fashion MNIST ([6] shows a 94.1% mean AUC), but not on the real-world data set MVTec AD (the method in [20] shows only 67% anomaly detection mean AUC on MVTec AD). However, a disadvantage of self-supervised learning methods is the significantly larger number of samples needed for training and testing. Since their methods augment by almost 100 times the amount of training and testing data (resulting in significantly longer running times), we consider that their approaches follow a different experimental setup than what is currently used in the field [1, 6, 8, 20, 53, 60, 73], and for this reason, we do not include their results in our tables. Moreover, self-supervised learning approaches do not seem to work well for anomaly localisation, especially for real-world anomaly images, such as the ones on MVTec AD. Nevertheless, even with the issues mentioned above, we plan to investigate further the potential of self-supervised pre-training in unsupervised anomaly detection and localisation.

References

[1] Davide Abati, Angelo Porrello, Simone Calderara, and Rita Cucchiara. Latent space autoregression for novelty detection. In *Proceedings of the IEEE Conference on Computer Vision and Pattern Recognition*, pages 481–490, 2019. [2](#), [5](#), [6](#), [7](#), [8](#)

[2] Samet Akcay, Amir Atapour-Abarghouei, and Toby P Breckon. Ganomaly: Semi-supervised anomaly detection via adversarial training. In *Asian conference on computer vision*, pages 622–637. Springer, 2018. [3](#), [8](#)

[3] Samet Akçay, Amir Atapour-Abarghouei, and Toby P Breckon. Skip-ganomaly: Skip connected and adversarially trained encoder-decoder anomaly detection. In *2019 International Joint Conference on Neural Networks (IJCNN)*, pages 1–8. IEEE, 2019. [8](#)

[4] Arslan Basharat, Alexei Gritai, and Mubarak Shah. Learning object motion patterns for anomaly detection and improved object detection. In *2008 IEEE Conference on Computer Vision and Pattern Recognition*, pages 1–8. IEEE, 2008. [2](#)

[5] Christoph Baur, Benedikt Wiestler, Shadi Albarqouni, and Nassir Navab. Deep autoencoding models for unsupervised anomaly segmentation in brain mr images. In *International MICCAI Brainlesion Workshop*, pages 161–169. Springer, 2018. [3](#)

[6] Liron Bergman and Yedid Hoshen. Classification-based anomaly detection for general data. *arXiv preprint arXiv:2005.02359*, 2020. [1](#), [2](#), [5](#), [8](#)

[7] Paul Bergmann, Michael Fauser, David Sattlegger, and Carsten Steger. Mvtac ad-a comprehensive real-world dataset for unsupervised anomaly detection. In *Proceedings of the IEEE Conference on Computer Vision and Pattern Recognition*, pages 9592–9600, 2019. [1](#), [2](#), [3](#), [4](#), [5](#)

[8] Paul Bergmann, Michael Fauser, David Sattlegger, and Carsten Steger. Uninformed students: Student-teacher anomaly detection with discriminative latent embeddings. In *Proceedings of the IEEE/CVF Conference on Computer Vision and Pattern Recognition*, pages 4183–4192, 2020. [1](#), [2](#), [3](#), [5](#), [6](#), [8](#)

[9] Paul Bergmann, Sindy Löwe, Michael Fauser, David Sattlegger, and Carsten Steger. Improving unsupervised defect segmentation by applying structural similarity to autoencoders. *arXiv preprint arXiv:1807.02011*, 2018. [1](#), [2](#), [3](#), [4](#), [8](#)

[10] David Berthelot, Colin Raffel, Aurko Roy, and Ian Goodfellow. Understanding and improving interpolation in autoencoders via an adversarial regularizer. *arXiv preprint arXiv:1807.07543*, 2018. [2](#), [4](#), [6](#)

[11] Christopher M Bishop. *Pattern recognition and machine learning*. Springer, 2006. [6](#)

[12] Philippe Burlina, Neil Joshi, and I-Jeng Wang. Where’s wally now? deep generative and discriminative embeddings for novelty detection. In *Proceedings of the IEEE/CVF Conference on Computer Vision and Pattern Recognition (CVPR)*, June 2019. [2](#)

[13] Kai-Wen Cheng, Yie-Tarng Chen, and Wen-Hsien Fang. Video anomaly detection and localization using hierarchical feature representation and gaussian process regression. In *Proceedings of the IEEE Conference on Computer Vision and Pattern Recognition (CVPR)*, June 2015. [2](#)

[14] Lucas Deecke, Robert Vandermeulen, Lukas Ruff, Stephan Mandt, and Marius Kloft. Image anomaly detection with generative adversarial networks. In *Joint european conference on machine learning and knowledge discovery in databases*, pages 3–17. Springer, 2018. [5](#), [6](#)

[15] David Dehaene, Oriel Frigo, Sébastien Combexelle, and Pierre Eline. Iterative energy-based projection on a normal data manifold for anomaly localization. *arXiv preprint arXiv:2002.03734*, 2020. [6](#), [7](#), [8](#)

[16] Allison Del Giorno, J Andrew Bagnell, and Martial Hebert. A discriminative framework for anomaly detection in large videos. In *European Conference on Computer Vision*, pages 334–349. Springer, 2016. [2](#)

[17] Arthur P Dempster, Nan M Laird, and Donald B Rubin. Maximum likelihood from incomplete data via the em algorithm. *Journal of the Royal Statistical Society: Series B (Methodological)*, 39(1):1–22, 1977. [4](#)

[18] Jia Deng, Wei Dong, Richard Socher, Li-Jia Li, Kai Li, and Li Fei-Fei. Imagenet: A large-scale hierarchical image database. In *2009 IEEE conference on computer vision and pattern recognition*, pages 248–255. Ieee, 2009. [2](#), [5](#), [6](#)

[19] Clément Godard, Oisin Mac Aodha, and Gabriel J Brostow. Unsupervised monocular depth estimation with left-right consistency. In *Proceedings of the IEEE Conference on Computer Vision and Pattern Recognition*, pages 270–279, 2017. [6](#)

[20] Izhak Golan and Ran El-Yaniv. Deep anomaly detection using geometric transformations. In *Advances in Neural Information Processing Systems*, pages 9758–9769, 2018. [1](#), [2](#), [5](#), [8](#)

[21] Dong Gong, Lingqiao Liu, Vuong Le, Budhaditya Saha, Moussa Reda Mansour, Svetha Venkatesh, and Anton van den Hengel. Memorizing normality to detect anomaly: Memory-augmented deep autoencoder for unsupervised anomaly detection. In *Proceedings of the IEEE International Conference on Computer Vision*, pages 1705–1714, 2019. [1](#), [2](#), [4](#), [5](#), [6](#)

[22] Jianping Gou, Baosheng Yu, Stephen John Maybank, and Dacheng Tao. Knowledge distillation: A survey. *arXiv preprint arXiv:2006.05525*, 2020. [5](#)

[23] Ishaan Gulrajani, Faruk Ahmed, Martin Arjovsky, Vincent Dumoulin, and Aaron C Courville. Improved training of wasserstein gans. In *Advances in neural information processing systems*, pages 5767–5777, 2017. [6](#)

[24] Raia Hadsell, Sumit Chopra, and Yann LeCun. Dimensionality reduction by learning an invariant mapping. In *2006 IEEE Computer Society Conference on Computer Vision and Pattern Recognition (CVPR’06)*, volume 2, pages 1735–1742. IEEE, 2006. [6](#), [8](#)

[25] Mahmudul Hasan, Jonghyun Choi, Jan Neumann, Amit K Roy-Chowdhury, and Larry S Davis. Learning temporal regularity in video sequences. In *Proceedings of the IEEE conference on computer vision and pattern recognition*, pages 733–742, 2016. [1](#)

[26] Kaiming He, Xiangyu Zhang, Shaoqing Ren, and Jian Sun. Deep residual learning for image recognition. In *Proceedings of the IEEE conference on computer vision and pattern recognition*, pages 770–778, 2016. 6

[27] Kaiming He, Xiangyu Zhang, Shaoqing Ren, and Jian Sun. Identity mappings in deep residual networks. In *European conference on computer vision*, pages 630–645. Springer, 2016. 6

[28] Ryota Hinami, Tao Mei, and Shin’ichi Satoh. Joint detection and recounting of abnormal events by learning deep generic knowledge. In *Proceedings of the IEEE International Conference on Computer Vision*, pages 3619–3627, 2017. 1

[29] Geoffrey Hinton, Oriol Vinyals, and Jeff Dean. Distilling the knowledge in a neural network. *arXiv preprint arXiv:1503.02531*, 2015. 5

[30] Radu Tudor Ionescu, Fahad Shahbaz Khan, Mariana-Iuliana Georgescu, and Ling Shao. Object-centric auto-encoders and dummy anomalies for abnormal event detection in video. In *Proceedings of the IEEE Conference on Computer Vision and Pattern Recognition*, pages 7842–7851, 2019. 1, 2, 4

[31] Diederik P Kingma and Jimmy Ba. Adam: A method for stochastic optimization. *arXiv preprint arXiv:1412.6980*, 2014. 6

[32] Diederik P Kingma and Max Welling. Auto-encoding variational bayes. *arXiv preprint arXiv:1312.6114*, 2013. 6

[33] Alex Krizhevsky, Vinod Nair, and Geoffrey Hinton. The cifar-10 dataset. *online: http://www.cs.toronto.edu/kriz/cifar.html*, 55, 2014. 1, 2, 5

[34] Gukyeong Kwon, Mohit Prabhushankar, Dogancan Temel, and Ghassan AlRegib. Backpropagated gradient representations for anomaly detection, 2020. 1, 2, 6

[35] Yann LeCun, Corinna Cortes, and CJ Burges. Mnist handwritten digit database. 2010. 2, 5

[36] Liu Li, Mai Xu, Xiaofei Wang, Lai Jiang, and Hanruo Liu. Attention based glaucoma detection: A large-scale database and cnn model. In *Proceedings of the IEEE/CVF Conference on Computer Vision and Pattern Recognition (CVPR)*, June 2019. 3

[37] Xiaoyan Li, Iluju Kiringa, Tet Yeap, Xiaodan Zhu, and Yifeng Li. Exploring deep anomaly detection methods based on capsule net. In *Canadian Conference on Artificial Intelligence*, pages 375–387. Springer, 2020. 6

[38] Wenqian Liu, Runze Li, Meng Zheng, Srikrishna Karanam, Ziyan Wu, Bir Bhanu, Richard J Radke, and Octavia Camps. Towards visually explaining variational autoencoders. In *Proceedings of the IEEE/CVF Conference on Computer Vision and Pattern Recognition*, pages 8642–8651, 2020. 8

[39] Wen Liu, Weixin Luo, Dongze Lian, and Shenghua Gao. Future frame prediction for anomaly detection—a new baseline. In *Proceedings of the IEEE Conference on Computer Vision and Pattern Recognition*, pages 6536–6545, 2018. 1, 2

[40] Yuyuan Liu, Yu Tian, Gabriel Maicas, Leonardo ZCT Pu, Rajvinder Singh, Johan W Verjans, and Gustavo Carneiro. Photoshopping colonoscopy video frames. *arXiv preprint arXiv:1910.10345*, 2019. 3

[41] Yuyuan Liu, Yu Tian, Gabriel Maicas, Leonardo Zorron Cheng Tao Pu, Rajvinder Singh, Johan W Verjans, and Gustavo Carneiro. Photoshopping colonoscopy video frames. In *2020 IEEE 17th International Symposium on Biomedical Imaging (ISBI)*, pages 1–5. IEEE, 2020. 1

[42] Ziwei Liu, Ping Luo, Xiaogang Wang, and Xiaoou Tang. Large-scale celebfaces attributes (celeba) dataset. 2, 6

[43] Weixin Luo, Wen Liu, and Shenghua Gao. A revisit of sparse coding based anomaly detection in stacked rnn framework. In *Proceedings of the IEEE International Conference on Computer Vision*, pages 341–349, 2017. 1

[44] Amir Markovitz, Gilad Sharir, Itamar Friedman, Lihi Zelnik-Manor, and Shai Avidan. Graph embedded pose clustering for anomaly detection. In *IEEE/CVF Conference on Computer Vision and Pattern Recognition (CVPR)*, June 2020. 2

[45] Gérard Medioni, Isaac Cohen, François Brémond, Somboon Hongeng, and Ramakant Nevatia. Event detection and analysis from video streams. *IEEE Transactions on pattern analysis and machine intelligence*, 23(8):873–889, 2001. 2

[46] Romero Morais, Vuong Le, Truyen Tran, Budhaditya Saha, Moussa Mansour, and Svetha Venkatesh. Learning regularity in skeleton trajectories for anomaly detection in videos. In *Proceedings of the IEEE Conference on Computer Vision and Pattern Recognition*, pages 11996–12004, 2019. 1, 2

[47] Gerhard Münz, Sa Li, and Georg Carle. Traffic anomaly detection using k-means clustering. 1

[48] Trong-Nguyen Nguyen and Jean Meunier. Anomaly detection in video sequence with appearance-motion correspondence. In *Proceedings of the IEEE International Conference on Computer Vision*, pages 1273–1283, 2019. 1, 2

[49] Guansong Pang, Chunhua Shen, Longbing Cao, and Anton van den Hengel. Deep learning for anomaly detection: A review. *arXiv preprint arXiv:2007.02500*, 2020. 1, 2

[50] Hyunjong Park, Jongyoun Noh, and Bumsup Ham. Learning memory-guided normality for anomaly detection. In *IEEE/CVF Conference on Computer Vision and Pattern Recognition (CVPR)*, June 2020. 2

[51] Adam Paszke, Sam Gross, Francisco Massa, Adam Lerer, James Bradbury, Gregory Chanan, Trevor Killeen, Zeming Lin, Natalia Gimelshein, Luca Antiga, Alban Desmaison, Andreas Kopf, Edward Yang, Zachary DeVito, Martin Raison, Alykhan Tejani, Sasan Chilamkurthy, Benoit Steiner, Lu Fang, Junjie Bai, and Soumith Chintala. Pytorch: An imperative style, high-performance deep learning library. In H. Wallach, H. Larochelle, A. Beygelzimer, F. d’Alché-Buc, E. Fox, and R. Garnett, editors, *Advances in Neural Information Processing Systems 32*, pages 8024–8035. Curran Associates, Inc., 2019. 6

[52] Deepak Pathak, Abhijit Sharang, and Amitabha Mukerjee. Anomaly localization in topic-based analysis of surveillance videos. In *2015 IEEE Winter Conference on Applications of Computer Vision*, pages 389–395. IEEE, 2015. 3

[53] Pramuditha Perera, Ramesh Nallapati, and Bing Xiang. Ogan: One-class novelty detection using gans with constrained latent representations. In *Proceedings of the IEEE Conference on Computer Vision and Pattern Recognition*, pages 2898–2906, 2019. 1, 2, 5, 6, 8

[54] Gunnar Rätsch, Bernhard Schölkopf, Sebastian Mika, and Klaus-Robert Müller. *SVM and boosting: One class*. GMD-Forschungszentrum Informationstechnik, 2000. 1

[55] Mahdyar Ravanbakhsh, Moin Nabi, Hossein Mousavi, Enver Sangineto, and Nicu Sebe. Plug-and-play cnn for crowd motion analysis: An application in abnormal event detection. In *2018 IEEE Winter Conference on Applications of Computer Vision (WACV)*, pages 1689–1698. IEEE, 2018. 1

[56] Mahdyar Ravanbakhsh, Moin Nabi, Enver Sangineto, Lucio Marcenaro, Carlo Regazzoni, and Nicu Sebe. Abnormal event detection in videos using generative adversarial nets. In *2017 IEEE International Conference on Image Processing (ICIP)*, pages 1577–1581. IEEE, 2017. 1

[57] Mahdyar Ravanbakhsh, Enver Sangineto, Moin Nabi, and Nicu Sebe. Training adversarial discriminators for cross-channel abnormal event detection in crowds. In *2019 IEEE Winter Conference on Applications of Computer Vision (WACV)*, pages 1896–1904. IEEE, 2019. 3

[58] Huamin Ren, Weifeng Liu, Søren Ingvor Olsen, Sergio Escalera, and Thomas B Moeslund. Unsupervised behavior-specific dictionary learning for abnormal event detection. In *BMVC*, pages 28–1, 2015. 1, 2, 4

[59] Olaf Ronneberger, Philipp Fischer, and Thomas Brox. U-net: Convolutional networks for biomedical image segmentation. In *International Conference on Medical image computing and computer-assisted intervention*, pages 234–241. Springer, 2015. 8

[60] Lukas Ruff, Robert Vandermeulen, Nico Goernitz, Lucas Deecke, Shoaib Ahmed Siddiqui, Alexander Binder, Emmanuel Müller, and Marius Kloft. Deep one-class classification. In *International conference on machine learning*, pages 4393–4402, 2018. 1, 2, 4, 5, 6, 7, 8

[61] Mohammad Sabokrou, Mohsen Fayyaz, Mahmood Fathy, and Reinhard Klette. Deep-cascade: Cascading 3d deep neural networks for fast anomaly detection and localization in crowded scenes. *IEEE Transactions on Image Processing*, 26(4):1992–2004, 2017. 1, 2

[62] Mohammad Sabokrou, Mohammad Khalooei, Mahmood Fathy, and Ehsan Adeli. Adversarially learned one-class classifier for novelty detection. In *Proceedings of the IEEE Conference on Computer Vision and Pattern Recognition*, pages 3379–3388, 2018. 1, 2, 8

[63] Thomas Schlegl, Philipp Seeböck, Sebastian M Waldstein, Georg Langs, and Ursula Schmidt-Erfurth. f-anogan: Fast unsupervised anomaly detection with generative adversarial networks. *Medical image analysis*, 54:30–44, 2019. 1, 3

[64] Thomas Schlegl, Philipp Seeböck, Sebastian M Waldstein, Ursula Schmidt-Erfurth, and Georg Langs. Unsupervised anomaly detection with generative adversarial networks to guide marker discovery. In *International conference on information processing in medical imaging*, pages 146–157. Springer, 2017. 1, 3, 6, 8

[65] Bernhard Schölkopf, John C Platt, John Shawe-Taylor, Alex J Smola, and Robert C Williamson. Estimating the support of a high-dimensional distribution. *Neural computation*, 13(7):1443–1471, 2001. 6

[66] Bernhard Schölkopf, Robert C Williamson, Alex J Smola, John Shawe-Taylor, and John C Platt. Support vector method for novelty detection. In *Advances in neural information processing systems*, pages 582–588, 2000. 2

[67] Waqas Sultani, Chen Chen, and Mubarak Shah. Real-world anomaly detection in surveillance videos. In *Proceedings of the IEEE Conference on Computer Vision and Pattern Recognition*, pages 6479–6488, 2018. 1, 2

[68] Ta-Wei Tang, Wei-Han Kuo, Jauh-Hsiang Lan, Chien-Fang Ding, Hakim Hsu, and Hong-Tsu Young. Anomaly detection neural network with dual auto-encoders gan and its industrial inspection applications. *Sensors*, 20(12):3336, 2020. 8

[69] David MJ Tax and Robert PW Duin. Support vector data description. *Machine learning*, 54(1):45–66, 2004. 2, 4

[70] Yu Tian, Gabriel Maicas, Leonardo Zorron Cheng Tao Pu, Rajvinder Singh, Johan W Verjans, and Gustavo Carneiro. Few-shot anomaly detection for polyp frames from colonoscopy. In *Medical Image Computing and Computer Assisted Intervention–MICCAI 2020: 23rd International Conference, Lima, Peru, October 4–8, 2020, Proceedings, Part VI 23*, pages 274–284. Springer, 2020. 1

[71] Yu Tian, Leonardo ZCT Pu, Rajvinder Singh, Alastair D Burt, and Gustavo Carneiro. One-stage five-class polyp detection and classification. In *2019 IEEE 16th International Symposium on Biomedical Imaging (ISBI 2019)*, pages 70–73. IEEE, 2019. 2

[72] Aaron Van den Oord, Nal Kalchbrenner, Lasse Espeholt, Oriol Vinyals, Alex Graves, et al. Conditional image generation with pixelcnn decoders. In *Advances in neural information processing systems*, pages 4790–4798, 2016. 6

[73] Shashanka Venkataraman, Kuan-Chuan Peng, Rajat Vikram Singh, and Abhijit Mahalanobis. Attention guided anomaly detection and localization in images. *arXiv preprint arXiv:1911.08616*, 2019. 1, 2, 3, 4, 5, 6, 7, 8

[74] Jue Wang and Anoop Cherian. Gods: Generalized one-class discriminative subspaces for anomaly detection. In *Proceedings of the IEEE International Conference on Computer Vision*, pages 8201–8211, 2019. 2

[75] Jiang Wang, Yang Song, Thomas Leung, Chuck Rosenberg, Jingbin Wang, James Philbin, Bo Chen, and Ying Wu. Learning fine-grained image similarity with deep ranking. In *Proceedings of the IEEE Conference on Computer Vision and Pattern Recognition*, pages 1386–1393, 2014. 2

[76] Zhou Wang, Alan C Bovik, Hamid R Sheikh, and Eero P Simoncelli. Image quality assessment: from error visibility to structural similarity. *IEEE transactions on image processing*, 13(4):600–612, 2004. 1, 2, 4, 6

[77] Zhou Wang, Eero P Simoncelli, and Alan C Bovik. Multi-scale structural similarity for image quality assessment. In *The Thirty-Seventh Asilomar Conference on Signals, Systems & Computers, 2003*, volume 2, pages 1398–1402. Ieee, 2003. 2, 4, 5, 6

[78] JiaYi Wei, JianFei Zhao, YanYun Zhao, and ZhiCheng Zhao. Unsupervised anomaly detection for traffic surveillance based on background modeling. In *Proceedings of the IEEE Conference on Computer Vision and Pattern Recognition Workshops*, pages 129–136, 2018. 1

[79] Lior Wolf, Sagie Benaim, and Tomer Galanti. Unsupervised learning of the set of local maxima. *arXiv preprint arXiv:2001.05026*, 2020. 6

- [80] Peng Wu, jing Liu, Yujia Shi, Yujia Sun, Fangtao Shao, Zhaoyang Wu, and Zhiwei Yang. Not only look, but also listen: Learning multimodal violence detection under weak supervision. In *European Conference on Computer Vision (ECCV)*, 2020. [1](#), [2](#)
- [81] Han Xiao, Kashif Rasul, and Roland Vollgraf. Fashion-mnist: a novel image dataset for benchmarking machine learning algorithms, 2017. [2](#), [5](#)
- [82] Dan Xu, Elisa Ricci, Yan Yan, Jingkuan Song, and Nicu Sebe. Learning deep representations of appearance and motion for anomalous event detection. *arXiv preprint arXiv:1510.01553*, 2015. [1](#), [2](#), [4](#)
- [83] Tianzhu Zhang, Hanqing Lu, and Stan Z Li. Learning semantic scene models by object classification and trajectory clustering. In *2009 IEEE conference on computer vision and pattern recognition*, pages 1940–1947. IEEE, 2009. [2](#)
- [84] Ying Zhang, Huchuan Lu, Lihe Zhang, Xiang Ruan, and Shun Sakai. Video anomaly detection based on locality sensitive hashing filters. *Pattern Recognition*, 59:302–311, 2016. [1](#)
- [85] Hang Zhao, Orazio Gallo, Iuri Frosio, and Jan Kautz. Loss functions for image restoration with neural networks. *IEEE Transactions on computational imaging*, 3(1):47–57, 2016. [6](#)
- [86] Jia-Xing Zhong, Nannan Li, Weijie Kong, Shan Liu, Thomas H Li, and Ge Li. Graph convolutional label noise cleaner: Train a plug-and-play action classifier for anomaly detection. In *Proceedings of the IEEE Conference on Computer Vision and Pattern Recognition*, pages 1237–1246, 2019. [1](#), [2](#)
- [87] Kang Zhou, Yuting Xiao, Jianlong Yang, Jun Cheng, Wen Liu, Weixin Luo, Zaiwang Gu, Jiang Liu, and Shenghua Gao. Encoding structure-texture relation with p-net for anomaly detection in retinal images. *arXiv preprint arXiv:2008.03632*, 2020. [2](#)
- [88] Bo Zong, Qi Song, Martin Renqiang Min, Wei Cheng, Cris-tian Lumezanu, Daeki Cho, and Haifeng Chen. Deep autoen-coding gaussian mixture model for unsupervised anomaly detection. In *International Conference on Learning Representations*, 2018. [2](#)